Proton NMR Characterization of Room-Temperature Aging after Modest Thermal Cycling in Isotactic Polypropylenes

D. L. VanderHart* and C. R. Snyder

Polymers Division, National Institute of Standards and Technology, Gaithersburg, Maryland 20899-8544

Received February 24, 2003; Revised Manuscript Received April 24, 2003

ABSTRACT: A proton NMR method, based on simple Bloch-decay spectra in the solid state, is presented that enables one to follow, with excellent sensitivity, structural changes associated with aging in semicrystalline polymers whose T_g is well below the aging temperature. The method is demonstrated for two representative isotactic polypropylene (iPP) samples, a Ziegler–Natta product and a metallocene product. Starting with samples that had been melt crystallized at a cooling rate of 1 °C/min and then aged at ambient temperature for long periods of time, subsequent mild heating cycles between ambient temperature and temperatures below 90 °C were applied. Such heating cycles remained more than 70 °C below the major crystalline melting temperature for iPP. Aging at 20 °C was monitored by NMR over aging times, 6 min < t_{age} < 4 d, following those heating cycles. It was shown that changes in the Bloch-decay spectra, corresponding to a lower limit of 2–3% of the mass of iPP being transformed from mobile to rigid components, accompanied the aging process over the 4 d period. Moreover, the time dependence was linear in log(t_{age}). It was further shown that the population of those noncrystalline (NC) stems with the highest mobility was most strongly reduced by aging; this observation does not, however, unambiguously establish that these same chains were the actual stems participating in the newly formed structures. The aging process was also shown to be reversible in the sense that the structures formed could be completely destroyed by repeating the mild heating cycle. Attention was paid to the definition of crystallinity, and an operational definition of crystallinity for the NMR measurements was based on the component with a long (>150 ms) value of T_{1xz}, the relaxation along the quantization axis of the toggling frame in a multiple pulse (MP) experiment. The complementary NC component, by this definition, includes not only the motionally averaged protons seen in the Bloch-decay spectrum but also certain protons with more hindered motions which, by Bloch-decay criteria, appear rigid. Approximately 75% of the NC protons transformed by aging are converted to "crystalline" protons, using the T_{1xz} definition; hence, the structural changes in aging seem to be dominated by crystallization, which we are comfortable to call secondary crystallization. A quick assay of the longitudinal proton relaxation, T_1^H, was also made during aging. Aside from some changes originating from oxygen losses during heating, T_1^H was found to be independent of aging time, and implications are pursued. Without making firm conclusions, observations are noted that may have relevance to the morphological location of secondary crystallites and to the factors that influence the amount of material available for such crystallization. The extent of secondary crystallization in the metallocene iPP is only modestly smaller than in the Ziegler–Natta iPP, although the metallocene iPP has a lower stereo–regiodefect concentration, a narrower polydispersity, and no expected "amorphous fraction". It is speculated that significant secondary crystallization would also characterize a defect-free iPP with low polydispersity.

Introduction

Isotactic polypropylene (iPP) is of great interest industrially for a variety of applications, e.g., as a neat polymer, as a component of a polymer blend, or as the matrix for a filled system. Polypropylene, like most synthetic polymers, does not completely crystallize when cooled from the melt. The presence of these amorphous or noncrystalline (NC) regions has been linked to changes in the mechanical properties at room temperature, e.g., in the work of Struik;[1–5] moreover, McCrum and co-workers[6,7] have also studied these changes extensively. The exact origin of the changes in iPP (and in other semicrystalline polymers) with aging time has been, and still is, in dispute.

In addition to the changes in the mechanical properties in a highly crystallized polymer, multiple melting endotherms are traditionally present; the lowest endotherm appears just above the annealing temperature, and its temperature and magnitude (total enthalpy) increase with logarithmic time. The nature of this peak

has been attributed to a variety of phenomena such as densification of the NC fraction (located between the lamellae, between the spherulitic fibrils, and/or between the spherulitic boundaries), crystallite perfection or densification, lamellar thickening, crystallization of impurities excluded by the crystal growth front, crystallization of constrained polymer chains forming small crystals or fringed micelles, and melting–recrystallization. One reason for the dispute lies in the inherent limitations of the techniques used to probe the structure of these materials. Differential scanning calorimetry (DSC) rarely provides similar values for crystallinity as other techniques,[8–10] and by necessity, the structures are destroyed by the scan; wide-angle X-ray diffraction (WAXD) requires an estimation of the amorphous halo and the lattice-imperfection factor;[11] and small-angle X-ray diffraction (SAXS) is extremely model dependent and requires estimation of the liquid scattering function.[12] It should be noted that the problems with SAXS analyses are enhanced in the case of iPP due to the crosshatched lamellar morphology[13] that is common to this material. Alamo and co-workers[8] demonstrated the

* Person to whom correspondence should be addressed.

differences in crystallinity measured by a variety of techniques for iPP. However, one feature that is generally agreed upon by most researchers as important for aging behavior is whether the annealing temperature is above or below the crystalline dielectric α_c relaxation. The crystalline α_c relaxation is most commonly associated with a rotation-translational motion traveling along the crystal stem (soliton)[14−22] which can draw from NC material in a crystal thickening process.

Marand and co-workers[23−25] have extensively examined what they believe to be a "secondary crystallization process" in a variety of polymers above and below the crystalline α_c relaxation temperature including poly(ethylene/1-octene random copolymers), poly(arylene ether ether ketone), and bisphenol A polycarbonate, poly(ethylene terephthalate). Additionally, they have examined the melting behavior of poly(butylene terephthalate), isotactic polypropylene, syndiotactic polypropylene, nylon-6, and ultrahigh molecular mass polyethylene and have determined that many of the features of this process are nearly universal for all semicrystalline polymers. From their measurements, they concluded that the measured change in the glass transition and the changes in the low endotherm with secondary crystallization are due to the decrease in the conformational entropy of the NC fraction as a result of the secondary crystallization processes. However, they allow for the fact that their results are also consistent with a change in the lateral dimensions of the secondary crystallites with crystallization time.

Because noncrystalline iPP has a glass transition temperature T_g around 0 °C,[1] thermally activated molecular reorganization can still induce further crystallization at room temperature even in highly crystallized samples. Furthermore, because the crystalline α_c relaxation for iPP is above 100 °C,[26] there is a wide window for studying this lower-temperature aging in which lamellar thickening should be negligible. In fact, the molecular nature of this aging behavior in iPP has previously been studied. For example, Agarwal and Schultz[27] used a combination of dynamical mechanical measurements, dilatometry, SAXS and WAXD, infrared (IR) spectroscopy, and NMR spectroscopy. They concluded that the physical aging in iPP is due to increasing constraint on the mobile NC fraction with no increase in crystallinity. Similarly, Yue and Msuya[28] compared the results of yield tests to the changes in crystallinity observed by DSC. They also concluded that within the experimental uncertainty that the degree of crystallinity did not change upon aging from 1 to 100 d and therefore some other molecular rearrangement rather than secondary crystallization was the cause of the increase in yield stress with aging time.

The purpose of this paper is 2-fold: (1) to present an NMR-based technique capable of measuring small increases in crystallinity and (2) to present the results of this technique as it applies to the room temperature annealing of isotactic polypropylene to help resolve some of the uncertainties associated with prior measurements. The use of NMR in examining crystallinity is not new; many papers can be found in the literature on the topic. However, the tracking of small changes in crystallinity by NMR is new. Specifically for iPP, as mentioned previously, Agarwal and Schultz[27] examined the microstructural changes in iPP with a variety of techniques including NMR, and more recently, Peemoeller and co-workers[29] used 2D time-domain ¹H NMR to

investigate annealed iPP over a temperature range of −120 to +120 °C.

Experimental Section

1. Samples and Heat Treatments. Two isotactic polypropylene (iPP) samples were used. One sample, designated iPP-1, is a commercial Ziegler−Natta-catalyzed iPP, marketed under the name Pro-fax 6523[30] and manufactured by Basell. The other sample, designated iPP-2, is a noncommercial metallocene-catalyzed sample that one of us had used in a previous study.[31] It was reported to have a mass-averaged relative molecular mass, M_w, of 200 500 g/mol, a polydispersity of about 2, and a defect content of 0.41 mol % of 2,1 regio (erythro) defects (and no detectable stereodefects) as characterized by solution-state NMR. Since we had no available molecular-mass information about iPP-1 and since the observed behavior of these samples was somewhat different, as will be seen, we felt that we needed to understand more about the differences in molecular mass. Thus, we performed gel permeation chromatography (GPC) on both iPP-1 and iPP-2, mainly for comparative purposes. Using poly(styrene) and poly(ethylene) mass-calibration standards, a universal calibration, and Mark Houwink constants of $K = 0.019$ mL/g and $\alpha = 0.725$,[32] we obtained the following values: for iPP-1, a number-averaged relative molecular mass, M_n, of 78 000 g/mol and a mass-averaged relative molecular mass, M_w, of 355 000 g/mol; for iPP-2, $M_n = 107\,000$ g/mol and $M_w = 206\,000$ g/mol. Considering our lack of iPP calibration standards, we consider the latter numbers to be in good agreement with those previously reported; for this paper, however, the important issue is the more precisely determined *comparative* characteristics of iPP-1 and iPP-2. While both have similar M_n values, their polydispersities, M_w/M_n (1.9 for iPP-2 and 4.5 for iPP-1), are very dissimilar. We also mention that the iPP-1 has a very weak peak ($<0.2\%$ of the main peak), which, if it belonged to an iPP molecule (as opposed to some additive), would have a molecular mass in the 400−600 g/mol range.

Both samples were initially melted into a plug under vacuum inside a 7 mm i.d. tube. Then the tube was sealed under nitrogen, remelted in an oven (195 °C) and finally crystallized at a cooling rate of 1 °C/min. The sample was then machined into a cylinder, 4 mm o.d. and 4 mm high for iPP-1 and 3 mm high for iPP-2.

The iPP-1 sample was the first that was investigated for aging effects. As we indicate in the next section, we did not embark on this research project with the idea of conducting a comprehensive study of aging in iPP. Hence, we were not initially very selective about the choice of sample or the temperature of thermal treatment marking the beginning of the aging time.

The thermal history of sample iPP-1 is as follows: after about 1 month of aging at ambient temperature, following melt crystallization, this sample was placed into an evacuated tube (no dimensional constraints) at 85 ± 5 °C for 40 h. Immediately after removal from the heated chamber, the sample was transferred in air to the sample rotor and placed into the magnet for the first measurement that commenced 6 min after removal. Measurements (at 20 ± 2 °C) were repeated at roughly logarithmically spaced intervals. The sample was not removed from the probe for the 4 days of the first aging experiment. Following this first 4 days of data taking, the sample was removed from the magnet and sat in the laboratory at ambient conditions (25 ± 2 °C) for nearly 8 months. Prompted by further questions about the aging process, we then reheated the sample to 69 ± 1 °C in air for 6 min and resumed the NMR aging measurements over a 4 d period. After this, we immediately heated the sample in air to 89 ± 1 °C for 6 min and then followed the aging behavior for another 3 d.

To address the remaining questions, especially those dealing with the reversibility of the aging phenomena and the possible role of chains with differing concentrations of defects, we chose the iPP-2 sample because it was well characterized and had a low, and uniform distribution of defects. It had aged for 49

months at 25 °C following melt crystallization. After performing some preliminary measurements on this aged sample, it was heated for 6 min at 89 ± 1 °C and aging was followed over a 4 d period. Then the same heating cycle was repeated and aging was followed for another 4 days. In each of these separate aging experiments, the sample was left in the probe in the magnet.

2. DSC. Differential scanning calorimetry (DSC) measurements were obtained on a Perkin-Elmer DSC-2C. Crystallization temperatures were calibrated against high purity (>99.999%) indium and tin standards at a heating rate of 0.31 °C/min and measured temperatures and enthalpies were calibrated against the same standards at a heating rate of 10 °C/min. Crystallinity was determined using 2-mg iPP samples; in contrast, aging, for sensitivity reasons, was quantified with larger samples (15 mg to 33 mg). The heat of fusion, ΔH_f, of 100% crystalline polypropylene determined by the diluent method is 209.2 J/g; however, it should be noted that Alamo and co-workers suggest that this method provides inaccurate values for iPP.[8] Lacking a better estimate, we will use this value for good comparative but only semiquantitative absolute crystallinity estimates.

3. NMR Measurements. All proton NMR experiments were conducted at 7.05 T (300 MHz) and at 20 ± 2 °C on a Bruker Avance spectrometer (Bruker Biospin, Inc. of Billerica, MA) equipped with a magic-angle-spinning (MAS) probe built by Doty Scientific, Inc. of Columbia, SC. The probe has a very low background signal arising from proton sources other than the sample. Mainly Bloch-decay signals, i.e., responses to single-pulse excitations, were observed in the spectra reported herein. The MAS frequency was 2500 ± 20 Hz. Temperature was not controlled, and the pressures used for spinning were very modest, i.e., 210 to 220 mB for the drive air and 360 to 430 mB for the bearing air. The fact that the drive air could only be set in 10 mB intervals meant that the bearing pressure varied more widely in order to achieve a constant spinning rate. The variation of the bearing pressure has some influence on the reproducibility of the sample temperature, but at these low pressures, the effects are most likely to cause variations less than 2 °C.[33] However, within any single aging experiment, temperatures were constant as a result of the sample remaining in the probe. Radio frequency field strength corresponded to a nutation frequency of 167 kHz (1.5 μs 90° pulse).

Aging was monitored using equilibrium, Bloch-decay spectra, which we will designate as the "M_o" spectra. These were acquired by averaging 24 scans using delay times of 5 s for a total collection time of about 2 min. Actual receiver dead time was 2.5 μs; dwell time was 1 μs (spectral width of 500 kHz). Data sizes were 65536 points for the free-induction decays (FIDs) as well as the Fourier transformed (FT) spectra. Analog filter widths on the receiver/digitizer were wide open (at least 10 MHz) so that bandwidth was effectively determined by the probe. No linear phase correction was used in obtaining the FT spectra; only a zero-order correction was applied. Since our data analysis features the presentation of difference spectra, it is important that the parent spectra giving rise to these differences are uniform in dc-offset, gain, and phase. Over the waiting times between experiments, and for these few scans, the stability of the spectrometer becomes an issue. Observed to vary over 4 d periods are the transmitter gain (within ±4%), the receiver gain (within ±4%) and the zero-order phase correction (within ±3°). These latter two variations respectively show up as changes in total integrals and a lack of reflection symmetry with respect to the spectral center frequency in difference spectra. Changes in transmitter gain are adjusted for at the beginning of each acquisition by adjusting the rf gain to give a 180° pulse for a fixed pulse width. To compensate for the small variations in receiver gain and phase, spectra were first baseline-corrected for dc-offsets. Then they were carefully multiplied by a constant near unity in order to make all integrals the same (all difference integrals = 0); moreover, zero-order phase corrections, chosen to the nearest 0.02°, were applied to yield the most symmetric difference spectra.

At convenient times between the samplings of the M_o spectra, quick assays of the proton longitudinal relaxation time, $T_1{}^H$, were also made. The (180°−τ−90°−observe−T) inversion−recovery sequence[34] was used. By assuming that the initial state is a complete inversion of the equilibrium magnetization and that the recovery of the magnetization follows a single, exponential time dependence, a null in the recovering magnetization will be observed at a delay time, τ_{null} = $T_1{}^H/\ln 2$. As a function of aging time, τ_{age} values of τ_{null} were measured. Even though there may be some systematic error or approximation in determining $T_1{}^H$ from the foregoing relationship, the fractional changes in τ_{null} are expected to reflect accurately the fractional change in $T_1{}^H$. Since $T_1{}^H$ is sensitive to molecular motions in the vicinity of the Larmor frequency near 2×10^9 rad/s, aging processes that either reduce the number of noncrystalline chains or constrain them in a way that affects the amplitude and/or frequency of their motions can create a change in $T_1{}^H$. While we expect the rotating methyl groups in both the crystalline (CR) and noncrystalline (NC) regions to provide much of the motion in this frequency range, the NC methine and methylene protons should also provide contributions to $T_1{}^H$. Hence, if there is a significant change in the fraction of NC chains or their angular amplitudes of motion, a measurable change in $T_1{}^H$ could result. The presence of reabsorbed paramagnetic oxygen may also have a small impact on $T_1{}^H$, so, for vacuum-dried samples, one must be cautious about attributing all changes in $T_1{}^H$ to molecular dynamics. (That is why only the first heat treatment was in a vacuum.)

Finally, we also carried out a few multiple-pulse[35−37] (MP) experiments that were intended to examine issues of crystallinity change and the morphological origins of the changes in line shape that were accompanying the aging process. The MP aspects of these experiments centered around the idea of *relaxation under MP*. Using the MREV-8 MP sequence,[36,37] and with the proper prepulse and receiver phase, one can observe so-called T_{1xz} relaxation.[38] This relaxation in solids is similar to $T_{1\rho}{}^H$ relaxation in that it is primarily sensitive to motions in the mid-kHz regime. It differs, however, from $T_{1\rho}{}^H$ in that T_{1xz} relaxation takes place in the absence of spin diffusion[39] between protons on neighboring sites. Hence, to a first approximation, T_{1xz} represents the superposition of the T_{1xz} relaxation profiles of all protons. Since methyl motions are typically much faster than midkilohertz, the contribution of methyl-proton motions to T_{1xz} is not very large; hence, contrasting backbone motions in the CR and NC regions show up as significant differences in T_{1xz}. In fact, one can adopt a definition of crystallinity based on the relative strength of the longest-relaxing ($T_{1xz} \approx 150$ ms) component.

The MREV-8 cycle time was 39.6 μs using 1.5 μs 90° pulses and the resonance offset was about 5 kHz. Unless otherwise noted, T_{1xz} experiments were conducted using nonspinning samples and modest air flows (50 mB) to the bearing jets of the probe only. Static samples are generally used because spinning samples can create T_{1xz}-decay artifacts not related to molecular motion.[40] For instrumental reasons, the T_{1xz} decays were truncated after 1400 cycles (55.4 ms). When the entire decay is not observed, it is critical that one do the experiments in such a way that dc offsets in the receiver are nulled. We accomplished this by alternately adding and subtracting signals that are correlated with the presence or absence of an initial 180° pulse.

We used MP experiments for three purposes. First, we occasionally took T_{1xz} data at different aging times and compared the decays in order to see the changes in T_{1xz} that were accompanying the observed line shape changes. Second, we occasionally measured crystallinity using the definition of crystallinity just mentioned. Such an assay required two T_{1xz}-decay profiles, namely, the equilibrium, total T_{1xz} decay and the CR−T_{1xz} decay of only the longest-relaxing, CR component. The latter was obtained using what we will designate as a "T_{1xz}−T_{1xz}−SD" sequence[41] where in the first stage of the sequence, the CR magnetization is isolated using a partial (16 ms) T_{1xz} decay. At the end of this period, the remaining magnetization (in this case, only CR magnetization remains)

is stored as polarization alternately parallel and antiparallel to the applied magnetic field, $\mathbf{B}_0$. Following a short second stage, consisting of a 20 μs spin diffusion (SD) time, t_{sd}, the third, readout phase of the experiment begins. It consists of a full T_{1xz} decay of this CR magnetization. For the subsequent evaluation of crystallinity by T_{1xz}, the CR$-T_{1xz}$ curve was scaled to match the T_{1xz} amplitude at long time; then the crystallinity was taken to be the amplitude ratio of the CR$-T_{1xz}$ to T_{1xz} at $t = 0$. The difference of these two decays represents the T_{1xz} profile of the NC component, i.e., the NC$-T_{1xz}$. In the third MP experiment, designated "$T_{1xz}-$FID$-$SD", we used a minor variant of the second experiment in which the readout mode of the spin diffusion experiment was changed to a Bloch-decay instead of a T_{1xz} decay. Using a 20 μs spin diffusion time, this yields the "broadline" spectrum of the CR component. If longer values of t_{sd} are used in either SD experiment, one can monitor how long it takes to recover the equilibrium line shape or T_{1xz} decay. Such information gives one a better understanding of either the distances between the protons that give rise to the faster and slower T_{1xz} components or the spatial separation between protons responsible for different line shape components.

Results

Differential Scanning Calorimetry (DSC). DSC scans, aimed at determining crystallinity levels, were taken at a rate of 10 °C/min, covering the temperature range from 0 to 200 °C. Small samples of the original iPP's that were melt crystallized at a cooling rate of 1 °C/min were used. The iPP-1 and iPP-2 samples had been stored at ambient temperature, respectively, for 12 and 52 months and should have possessed extensive aging-induced crystallization. Such samples (2–3 mg range) are small enough to avoid possible superheating effects. The crystallinities of iPP-1 and iPP-2 were, respectively, found to be 0.43 and 0.50, based on a heat of fusion of 209.2 J/g for the pure crystal.[42,43] The DSC traces are shown in Figure 1.

A large, 34-mg sample of iPP-1 (the largest sample that would fit into the DSC pan) was used to demonstrate, at an aging time of 1 d, the observability by DSC of the aging process in iPP-1. An attempt to follow the aging process by DSC was not undertaken. The sample, originally crystallized at a cooling rate of 1 °C/min, was taken through several thermal cycles that are shown in the inset of Figure 2. Labels in the inset correspond to traces shown. The cooling rate used throughout ($r_2 = 20$ °C/min) was chosen to approximate the air cooling rate of the NMR samples. Prior to each scan, the sample was cooled momentarily to 0 °C in order to achieve signal stability over the range from 20 to 89 °C. In Figure 2, trace *a* is that of the empty pan and trace *b* shows the absence of any notable endotherm for a minimal aging time. Traces *c* and *d* show the reproducibility of the endotherm associated with an aging time of 24.5 h at 20 °C. Maxima in these latter traces occur at 45 °C, moreover the reproducibility of detail in these traces is striking. Estimates of the crystallinity that would be associated with such endotherms, using the baselines shown and assuming a ΔH_f of 209.2 J/g, are 0.57% ± 0.10% for trace *c* and 0.60% ± 0.10% for trace *d*. Similar runs were performed on a sample of iPP-2, and, following the 24.5 h aging at 89 °C, the crystallinity increase was estimated to be 0.32% ± 0.12%. The similarity of traces *c* and *d*, despite the different times spent at 89 °C, suggests that no appreciable aging is occurring at 89 °C. In addition, residing at 89 °C for at least 10 min is sufficient to destroy the population of aged structures that formed at 20 °C over a 24 h period. The latter observation leads us to conclude that if aging
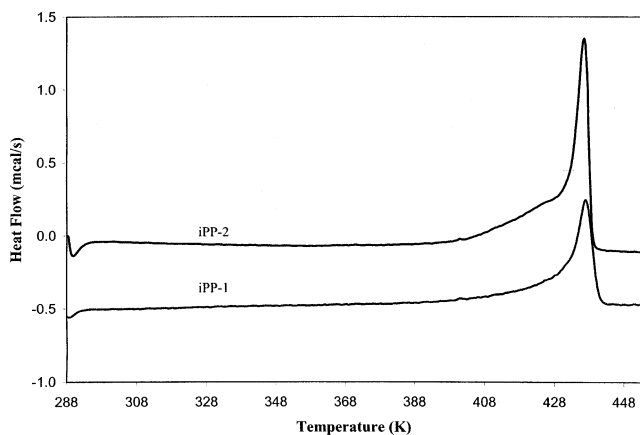
Figure 1. DSC heating traces showing crystalline melting endotherms. Endotherms are different in size because the iPP-2 sample size is about 50% larger than for iPP-1; moreover, the crystallinity of the former is higher.
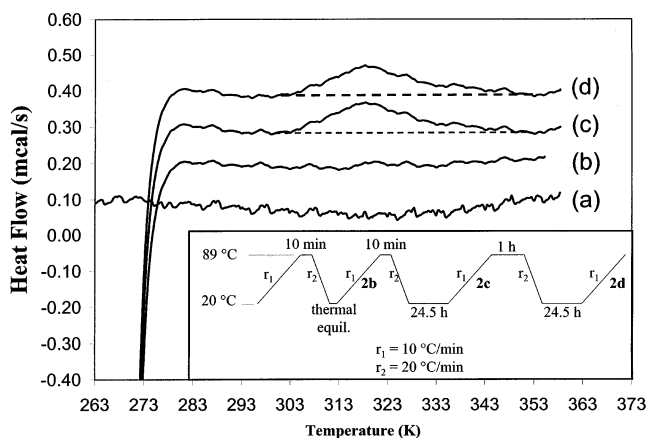
Figure 2. Linearly corrected DSC heating traces for an empty pan (a) and for one large 33.7-mg iPP-1 sample (b–d), initially melt crystallized at a cooling rate of 1 °C/min. Thermal histories for this sample are given in the inset and labels correspond to associated DSC curves. The temperature is dropped quickly to 0 °C just prior to each scan. Note the excellent reproducibility of curves c and d. The straight lines are drawn to aid the eye as probable baselines.

involves secondary crystallization, the size of such crystallites must be sufficiently small to melt at 89 °C.

NMR. 1. Perspectives. There are five main points that we wish to illustrate in presenting these data. First, we are claiming that when the noncrystalline (NC) chains of a polymer such as iPP are significantly above their reported glass transition temperature of about 0 °C, there is enough spectral motional narrowing, and sufficient contrast between the line shapes of the crystalline (CR) and NC chains so that, using changes in the proton NMR spectra, slow, room-temperature aging can be followed in time, both in a quantitative manner and with excellent sensitivity. Second, we present evidence that this aging involves a change of mobility where the dominant process is a conversion of NC to CR chains. Third, we recognize, as many others have, that the NC region of iPP does not have uniform mobility; thus, we will show that the population of most mobile chains is most strongly altered during aging. Fourth, we demonstrate the reversibility of this aging process. Finally, we will demonstrate that the number of chain segments involved in this crystallization grows approximately logarithmically in time over the 4 d period of our observation.
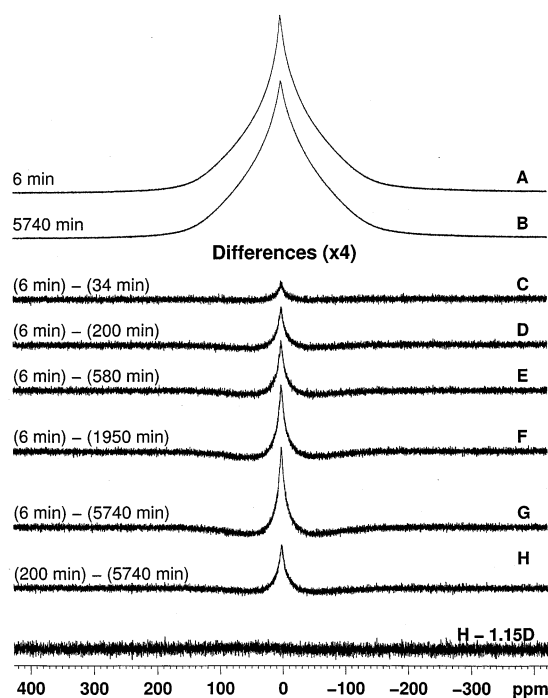
Figure 3. Bloch-decay spectra and difference spectra associated with a 4 d aging period for iPP-1. A, B: full spectra for t_{age} = 6 min and 4 d, respectively. C–H: vertically amplified (×4), zero-integral difference spectra involving spectra at the 2 indicated t_{age} values. Spectrum G = A − B. The lower spectrum is the indicated "difference of difference" spectrum illustrating that, within experimental error, the line shape changes over the first half of the aging-induced conversion are identical to those in the second half.

Since an important facet of this paper is the presentation of an NMR methodology useful for polymer characterization, it is helpful to recognize at the outset that the choice of the iPP-1 sample, its crystallization history, and its heat treatment at 89°C were NOT initially chosen as being especially significant in terms of an aging study of iPP. Rather, we had first noticed time-dependent line shapes after vacuum-drying a nanofilled iPP at 89 °C. Thus, the first iPP data were collected when we checked whether this behavior was characteristic of unfilled iPP. In retrospect, however, this choice of a thermal cycle is, we believe, still meaningful in terms of the polymer story represented. Our approach in presenting the aging related line shape results will be chronological, i.e., first iPP-1 and then iPP-2 results. The iPP-2 results pertain to a better-characterized sample. The results for iPP-2 also relate to the generality of the aging phenomenon since we avoid the question of whether the phenomena observed are associated only with the small fraction of more defective chains which tend to be present in iPP's synthesized with Ziegler–Natta catalysts.[44]

2. Aging Changes in Broadline Spectra. In Figure 3, spectra A and B are M_0 spectra of iPP-1 taken, respectively, at the shortest (6 min) and longest (5740 min) aging times, t_{age}, after initial vacuum-heating for 2 d at about 85 ± 5 °C. These line shapes are rather featureless, tentlike shapes, and it is not so clear from inspection that differences are significant. Qualitatively, for the CR contribution to these line shapes, the fact that half the protons on the iPP repeat unit are methyl protons that undergo partial line narrowing by rotating rapidly about their C_{3v} axes means that the line shape,

dominated by proton–proton dipolar interactions, will have more central intensity than would, e.g., the line shape for CR polyethylene. In addition, the NC segments that can undergo larger-amplitude motions than their CR counterparts will also see linenarrowing, probably more extensive than the CR methyl protons. Indeed, the relatively sharp cusp atop each line shape is an indication of some motional narrowing in the sample. Nevertheless, and importantly, there are no clear demarcations in line widths in Figure 3, parts A and B, that would form the basis for the clean separation of signals into CR and NC (rigid and motionally narrowed) contributions.

In Figure 3C–H, we display difference spectra, amplified vertically times 4. The paired τ_{age} values associated with each difference spectrum are indicated in the figure. Spectra C–G show differences with respect to the shortest t_{age}, and one sees spectra with increasingly strong, positive narrower features offset by increasingly strong, negative broader features. Recall that the total integral of each of these spectra is zero. The positive features represent spectral regions where aging causes intensity loss; the negative features represent intensity gains. Spectrum H is the difference spectrum associated with 200 min and the longest time of 5740 min (≈4 d). This spectrum is generated in an attempt to ask the question whether there is a steady loss of mobility in the NC region as aging progresses. If this were true, the NC segments, which lost mobility during the last half (mass-wise) of the aging process, would come from a more restricted state (wider line width) than would the material that lost mobility during the first half of the aging process. The difference spectrum given at the bottom of Figure 3 makes such a line shape comparison between first-half changes (spectrum D) and second-half changes (spectrum H). The result is that the narrow portions of the difference spectra are, within experimental error, the same; i.e., *there is no line shape evidence for a continuous restriction of the mobility with* τ_{age}.

In Figure 4, we address the issue of whether the observed line shape changes look like crystallization, or, for example, just a greater restriction in the amplitude of fast reorientational motions for NC segments. Of course, from a line shape point of view, this distinction is qualitative in the sense that the criterion of line width that we apply is more sensitive to the loss of angular amplitude of fast motions than it is to the precise organizational state or perfection in the solid, i.e., immobility on a time scale of 10^{-5} s is not necessarily equivalent to crystallization. In Figure 4B, we reproduce the difference of Figure 3G associated with the shortest and longest times. In Figure 4A, we give the M_0 spectrum, multiplied by 0.029. Figure 4C is the sum of parts A and B of Figure 4 and illustrates that the widest line shape features are completely nulled in this summed spectrum. This means that the line shape changes involved in aging include a growth of line shape features indistinguishable from the widest, i.e., the most rigid, CR segments. In other words, *it appears that aging involves crystallization*. We will find further verification for this claim from the MP results.

In Figure 5, we plot the growth of this component vs log τ_{age} (open triangles). Ordinate values are determined using the analysis illustrated in Figure 4; i.e., we use the difference spectrum, Figure 4B, as a reference spectrum that represents a conversion of material equal
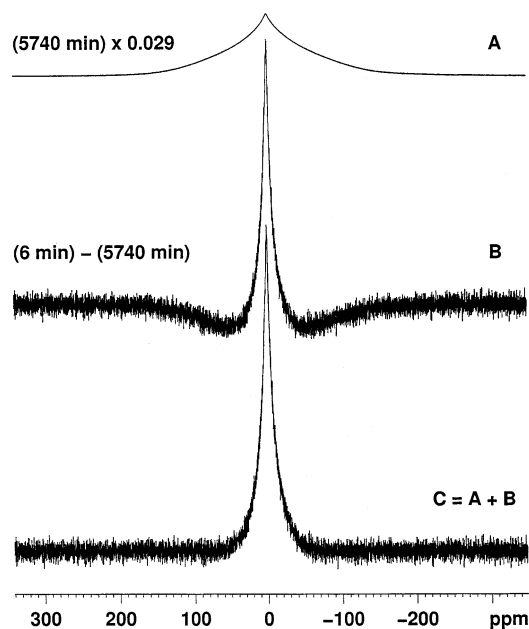
Figure 4. Spectra illustrating that the negative-going broad component of the difference spectra, illustrated by the difference spectrum, B (=Figure 3G), has a line width indistinguishable from the broadest component in the M_o spectrum (A) which is scaled by the factor of 0.029. Evidence for this is the flatness of the baseline in the region of the broad component in spectrum C (=A + B).
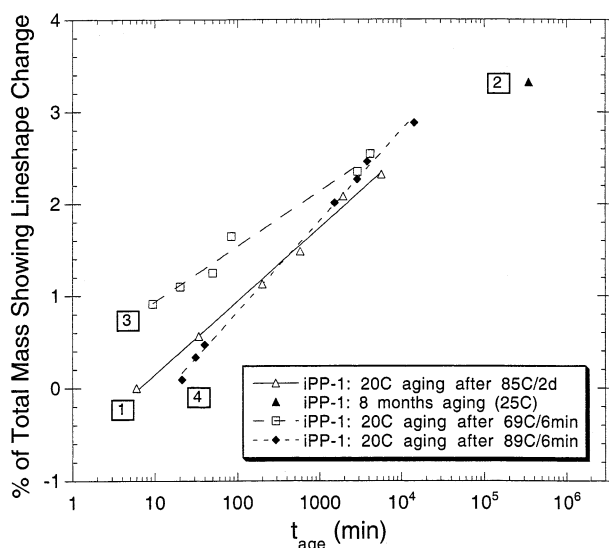
Figure 5. Percentages of the total mass showing line shape changes vs log(t_{age}) at 20 °C for iPP-1, the Ziegler–Natta polymerized sample. The legends define the initial thermal treatment and the numbered boxes in the figure indicate the sequence of thermal treatments. Note especially the linearity of these plots and the fact that thermal cycling to 69 °C does not create as strong an initial mobile fraction as does the subsequent heating to 89 °C. The "zero" level in this plot is taken, arbitrarily, to be the condition at the time of earliest sampling after the first heating cycle. Note also that the point representing the 8-month aging period represents aging at 25 °C, not 20 °C. Estimated standard uncertainties associated with each datum in this and Figures 6 and 7 is ±0.15%.

to 2.3% (= 0.029 × 0.78) of the entire sample. (As will be discussed later in connection with Figure 9, we have isolated the line shape of the rigid component and the latter accounts for 78% of the intensity in the M_o spectrum of Figure 4A.) Moreover, in Figure 5, we arbitrarily establish the ordinate "0" value to be that
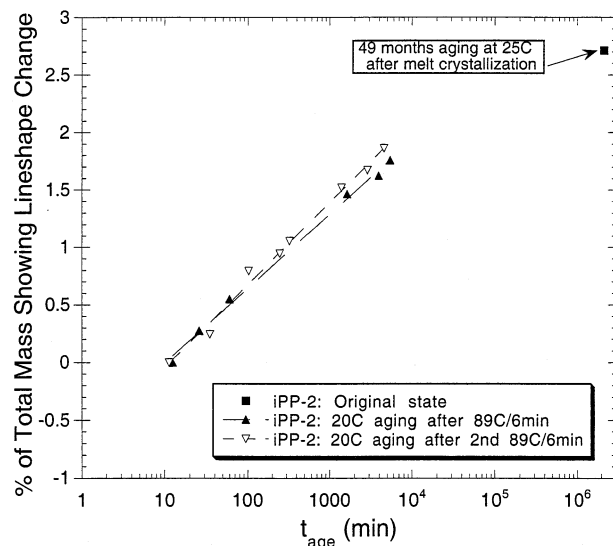
Figure 6. Plot, similar to Figure 5, for the metallocene polymerized iPP-2. Note that the thermal treatments are duplicated here and that the starting points are identical, indicating that a repetition of the heating cycle destroys all of the aging-induced structures formed after the first heating cycle.
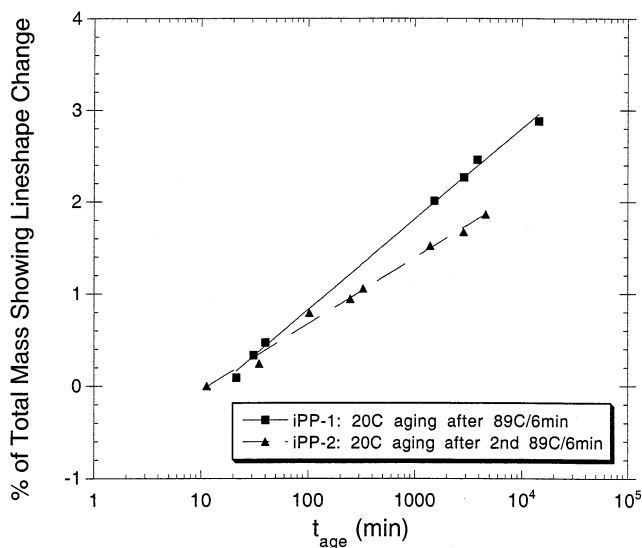
Figure 7. Contrast in amplitude of aging changes for iPP-1 and iPP-2 after heating cycles to 89 °C for 6 min. The slope for iPP-2 is about 72% that of iPP-1. The similarity of amplitudes at short aging times is a matter of the arbitrary assignment of the zero level in Figures 5 and 6; in actuality, the iPP-1 sample has, at early aging times, an excess of motionally narrowed intensity corresponding to 3.6% of the total intensity.

at the shortest observation time. Other difference spectra are then ratioed to this difference spectrum in order to determine the fractions converted. More aging data appear in Figure 5, and the numbered boxes in the figure along with the legend define the chronology of aging. In plotting the aging changes associated with the different thermal treatments, spectrum B in Figure 4 was still used as a reference for amplitude changes after suitable adjustments were made for any drift in the total integrals of the M_o spectra at the earliest aging times. Also, in Figure 5, the inequality of the ordinate values at the beginning of each aging run is based on line shape differences between the corresponding spectra. Unfortunately, we did not always manage to obtain our first
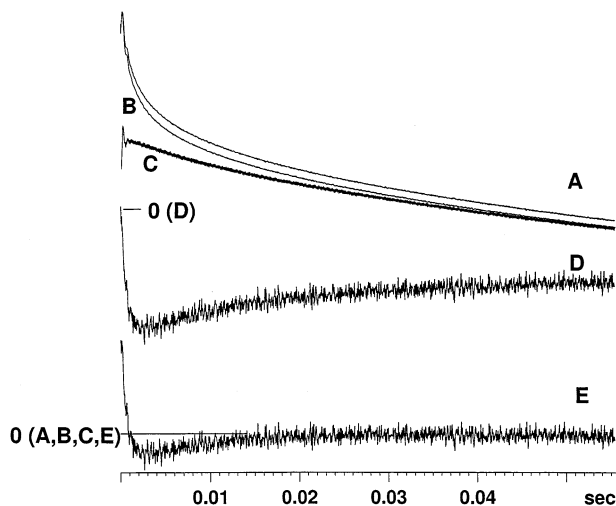
Figure 8. T_{1xz} decays and decay differences for the nonspinning iPP-2 sample with different aging histories. A: T_{1xz} for original sample, aged at 25 °C for 49 months. B: T_{1xz} for same sample 30 min after a heating cycle to 89 °C for 6 min. C: Rescaled decay for the "B" sample using the $T_{1xz}-T_{1xz}-SD$ experiment (16 ms of T_{1xz} preparation, short spin diffusion time = 20 μs). This experiment extracts the decay of the crystalline protons only. Rescaling is done to match the long-term decay of B. The ratio of initial intensities of C to B gives crystallinity (0.72 ± 0.03) and the difference, B − C (not shown) gives the T_{1xz} profile of the noncrystalline (NC) region. This NC decay is not single-exponential; instead, it can be broken down into one component with a T_{1xz} of 1 ms, 0.19 ± 0.02% and another component with a T_{1xz} in the 5−8 ms range, 0.09 ± 0.02%. The amplitude of the 1 ms component corresponds closely to the fraction of motionally averaged protons identified in the Bloch-decay spectrum. D = (A − B) × 10. This normalized difference starts at zero and goes quickly negative, indicating that B has a larger component with fast decay. The longer-time positive growth of D is truncated and indicates the presence of a long-T_{1xz} component, present in A, which the subsequent heating has destroyed. E is the difference, D, with a scaled fraction of C added so as to null the long-T_{1xz} component. Here one can more easily see that heating to 89 °C for 6 min has created an increase in the fastest-T_{1xz} component, and that this increase arises mainly 75−80% from the longest-T_{1xz} component and secondarily 20−25% from the intermediate-T_{1xz} component. Note the "zero" levels indicated for each curve.

spectrum at similar times. Nevertheless, within experimental error, over the 3−4 d periods of each study, *the conversion rate in this aging process, over times between 6 and 5000 min, is, within experimental error, linear in log(t_{age}). Moreover, the amount of material melted, or softened, is a function of the heat treatment temperature with a subsequent rate of change upon aging that depends on the amount that was melted.* We note that there was 8 months of aging in the laboratory between the end of the first aging run and the beginning of the second. Prior to the second heat treatment, we assayed the effect of aging over the 8 months. This point appears as a separate point in Figure 5. Note that this point is slightly below the extension of the curve through the "open-triangle" data. We know that the temperature of aging over the 8 months was slightly higher (≈4 °C) than that over the 4 d measurement time. If this were the reason for the deviation of the 8-month point from the slope of the 4 d growth data in Figure 5, the implication would be that growth would slow as one raised temperature. The latter conclusion would be consistent with a growth rate determined more by the energetics and thermal stability of the structures formed
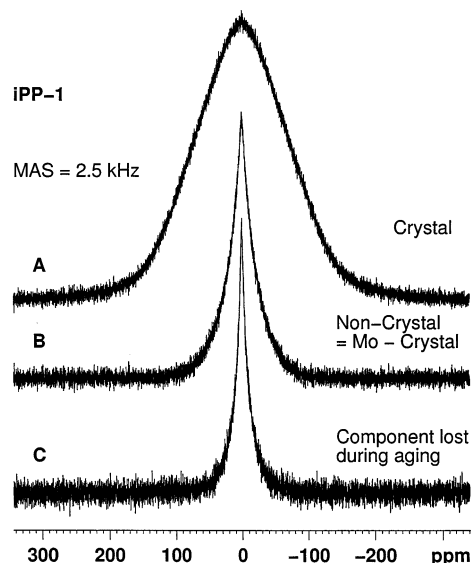
Figure 9. Different Bloch-decay line shape components for the iPP-1 sample at v_r = 2.5 kHz. A: crystalline line shape from the $T_{1xz}-FID-SD$ experiment with a 16 ms T_{1xz} preparation and a spin diffusion time of 20 μs. (This line shape also agrees very well with the line shape obtained using a nonspinning sample.) B: Spectrum of NC protons obtained by difference (=M_0 − kA where k is chosen to be a maximum, subject to the condition that no negative intensity is allowed). C: Spectrum of the narrow component lost in the aging process (same as Figure 4C). That aging preferentially changes the population of the more mobile protons in the NC region is possibly an indication that secondary crystallization is happening in regions more distant from crystal surfaces.

rather than the kinetics of the molecular rearrangements necessary to promote those structures. On the other hand, we observed that the difference line shape (not shown) associated with the M_0 spectrum of Figure 3B (t_{age} = 5740 min) and that after 8 months of aging, did not fully mimic the difference in Figure 4B. The average, narrower line width associated with the material that was converted at these long times was about 20% wider than in spectrum B in Figure 4. This observation is consistent with the idea that longer-term aging affects a population of chains that show slightly more constraint than did the population altered at earlier times.

In Figure 6, we show data, similar to Figure 5, for iPP-2. We first took a spectrum before any heat treatment; i.e., the sample had aged for 49 months in the laboratory following the original melt crystallization at a cooling rate of 1 °C/min. Then, followed 2 cycles of 89 °C heat treatments/4 d aging. Data agree with the DSC results for iPP-1 in that *aging is reversible, i.e., whatever structures were formed during the aging process following a heat treatment to 89 °C can be remelted by returning to the same heat treatment conditions.* Slight differences in slope in the two aging curves of Figure 6 may be related to slightly different probe temperatures owing to varied spinning-air pressures; we cannot monitor our probe temperature accurately enough to comment on this point. Two other conclusions also follow: (a) A comparison in Figure 7 of the magnitude of the changes in iPP-1 and iPP-2 for similar heat treatments shows that *the fractional changes over a 4 d aging time are about 40% larger in iPP-1 than iPP-2.* (This is also in agreement with the relative changes in enthalpy of fusion of the iPP-1 and iPP-2 after 1 d of aging, as measured by DSC.) (b) The datum in Figure

6 for the original, 49-month aged sample does not fall on the curve-fits for the 4 d aging. Again, we recognize that the two temperatures of aging were slightly different. Hence, we do not know at this time whether, at very long times, growth proportional to $\log(t_{age})$ is not sustained or whether this is an effect of a small increase in aging temperature over the long times.

3. Crystallinity Measures. As mentioned earlier, the Bloch-decay (broadline) spectrum does not show a well-defined distinction between the line widths of CR or NC protons. At the same time, the line width changes associated with aging involve line shape components with very significant line width differences (see spectrum B in Figure 4). In this section, we wish to isolate T_{1xz} decays as well as line shapes associated with the CR regions. We will also address the question of the best NMR assay for crystallinity.

We will first adopt a definition of crystallinity based on a separation of the long-T_{1xz} component. In other words, this definition of crystallinity features the fraction of protons with the lowest spectral density of motions in the midkilohertz region. Implementation of such a separation, based on the $T_{1xz}-T_{1xz}$-SD experiment, is shown in Figure 8 for sample iPP-2. Decay B is the truncated, T_{1xz} decay for all of the protons for t_{age} = 17 min following the 6 min heating at 89 °C. This decay consists of a rapid decay over the first few milliseconds followed by a much slower decay; the faster decay is ascribed to the NC regions. Decay C is the rescaled, T_{1xz} of only the CR magnetization at t_{age} = 32 min; i.e., this is the signal from the $T_{1xz}-T_{1xz}$-SD experiment with the initial T_{1xz} preparation period = 16 ms and t_{sd} = 20 μs. This spectrum is scaled so that the amplitude at 55.4 ms is equal to that of decay B. The "0" levels for these decays are indicated near the bottom of the figure. The decay B/C amplitude ratio at t_{sd} = 0 gives a measure of crystallinity which is 0.72 ± 0.03. This number would be more precise, were it not for the fact that at the earliest times, there is some ringing associated with the nonideality of the initial pulse; that is to say, the original magnetization is not exactly aligned with the "locking direction" in the toggling frame when the MP sequence is applied. Hence, the measurement of crystallinity, in this case, is based on projections of the nonoscillating portions of Figure 8B and Figure 8C to the time origin. Most of the uncertainty is in the extrapolation of decay B since there is a significant fast-decay component.

The difference decay, B − C, should correspond to the T_{1xz} decay of the NC protons assuming that Figure 8C is made up exclusively of contributions from CR protons. This NC decay (not shown) is nonexponential, consisting of a faster and an intermediate decay (see figure caption for Figure 8). The fraction of faster decay corresponds closely to the fraction of motionally averaged protons in the Bloch-decay line shape using analysis methods illustrated in Figure 9, strongly suggesting that the intermediate-decay component would appear "rigid" using a line width criterion. Further support for correspondences between the T_{1xz} behavior and the line widths comes from the observation (not shown) in a T_{1xz}-FID-SD experiment, using a 1 ms T_{1xz} preparation and a very short spin diffusion time, where the motionally narrowed component is more strongly attenuated and where there is no preferential selection of line widths within the motionally narrowed manifold.

We now turn to the question of how the Bloch-decay spectra reflect crystallinity. The fact that the CR regions should be the least mobile and provide the least line-narrowing motions implies that the broadest contributions of the methine, methylene and methyl protons should each be associated with the protons in the CR regions. At the same time, owing to fast methyl rotation about their C_{3v} axes, and the lack of geminal dipolar coupling for methine protons, the methylene protons will offer the broadest absolute line shape contribution to the overall CR line shape. Short of calculating the CR line shape from first principles, we choose rather to isolate the CR line shape using the T_{1xz}-FID-SD experiment, again using an initial T_{1xz} period of 16 ms and a t_{sd} of 20 μs. Results are shown in Figure 9 for the iPP-1 sample that had been aged for about 3d following the heat treatment at 69 °C. Spectrum A in Figure 9 is that of the CR regions and is obtained directly from this T_{1xz}-FID-SD experiment. Given that the T_{1xz} decays are the superposed individual decays of each proton, it is a fair question to ask whether the methyl, methine and methylene protons contribute equally to this CR line shape. We looked into this question briefly and concluded that, to a good approximation, they did. There are two related observations that support this conclusion. First, and most important, the line shape of the CR region varied only slightly in this T_{1xz}-FID-SD experiment when t_{sd} was extended to 1 ms. The latter is a time when nearly full equilibration is expected between protons on the same monomer. Second, if t_{sd} is allowed to vary between 0.02 and 100 ms in the $T_{1xz}-T_{1xz}$-SD experiment, we can plot the change in magnetization level of the CR region toward its sample average value (equal to the "0" level in Figure 10) against $t_{sd}^{1/2}$. The fact that the slope in Figure 10 is linear over the first millisecond of spin diffusion is again an indication that the 16 ms T_{1xz} preparation creates similar polarizations of all protons in the CR regions. If this were not true, there would be a steeper decrease of the data of Figure 10 over the first millisecond.

Incidentally, the other main deduction from Figure 10 is that the morphologies of iPP-1 and iPP-2 are very similar. If we interpret[40] the initial slopes in terms of the overall repeat distances characteristic of each morphology, and if we use a spin diffusion constant of 0.7 nm²/ms for both CR and NC regions along with respective crystallinities of 0.68 and 0.72, then the overall repeat distances (long periods) are 24 and 23 nm and the implied crystallite thickness is 16 nm. This similarity in overall repeat distances is not surprising, given the similar melt-crystallization histories.

Returning to Figure 9, spectrum B is that of the NC component in the following sense: If, in the M_0 line shape, *every monomer whose protons yield a line shape like 9A are CR monomers,* then, the remaining, protons, whose line shape contributions show some motional averaging, can be called NC. Thus, spectrum B in Figure 9 is generated by subtracting the maximum fraction of a component with the line shape of 9A from the M_0 line shape. Finally, spectrum C in Figure 9 is the same as spectrum C in Figure 4; i.e., this is the NC component that most strongly contributes to the aging changes.

The full widths at half-heights in Figure 9 are, respectively, 49 ± 2, 10.5 ± 0.7, and 4.3 ± 0.2 kHz. Hence, a very qualitative comment is that *aging alters the mobility of that population of NC monomers that exhibit the higher mobilities*. Note that this is *not*
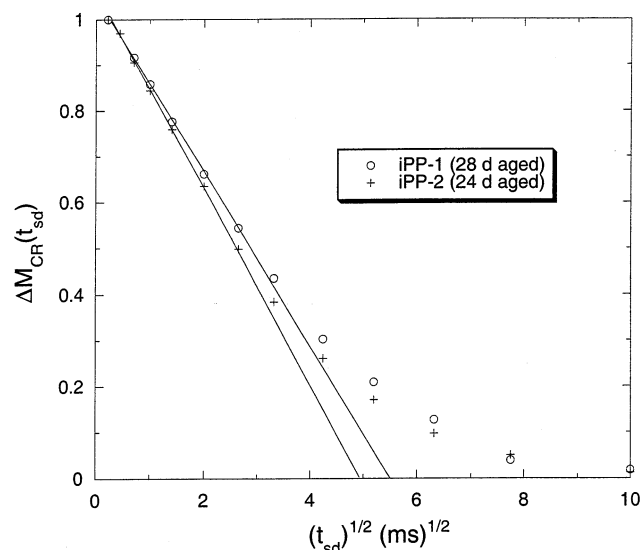
Figure 10. Spin diffusion plots for similarly aged iPP-1 and iPP-2 based on nonspinning $T_{1xz}-T_{1xz}$–SD experiments using variable spin diffusion times, t_{sd}. The preparation is the selection of crystalline magnetization using 16 ms of T_{1xz}. The ordinate measures the relative decrease in the CR magnetization vs $t_{sd}^{0.5}$ with unity representing the CR magnetization at very short SD times and zero representing the CR magnetization when the polarization of all regions is equal (internal spin equilibrium). Straight line are drawn to indicate initial slopes. The intercepts of these lines with the abscissa give characteristic times which can be used, in conjunction with crystallinity values, to estimate long periods (23 nm for iPP-2 and 24 nm for iPP-1). Thus, morphologies of iPP-1 and iPP-2, by this measure, are very similar. Also, the slope linearity at short times indicates that in the CR regions, all protons, including the methyl protons, have very long T_{1xz}'s.

equivalent to claiming that the rigidifying monomers in the aging process are *exclusively drawn* from the pool of more mobile NC monomers. For example, in the model where (a) there is a distribution of NC mobilities and line widths and (b) aging causes all NC segments to slow somewhat, the population that would *appear to be* decimated would be the most mobile population, since that is the population that cannot be replenished by a general reduction in NC mobility. There is also a corollary statement that relates to the *deduced fraction* of protons whose mobilities are modified by aging: *Only when proton line shapes consist of only two components can difference spectra be analyzed with confidence in terms of the fraction of residues whose mobilities are transformed by aging. If more than two components are present, then the amplitudes in the difference spectra correspond to the minimum fraction of chains whose mobilities are altered.* Thus, in Figures 5–7, the ordinate values are to be understood as minimum values since we do not wish to insist that all motion in the NC region is uniformly constrained.

There is an important perspective about the CR fraction that derives from the relative integrals of spectra A and B in Figure 9. As fractions of the total M_0 intensity, line shapes A and B in Figure 9 respectively represent 77% and 22%. Given that, in this sample, the $T_{1xz}-T_{1xz}$–SD evaluation of crystallinity was 68%, the implication is that about 10% of the monomers in this iPP-1 sample have protons which are quite rigid from a line width point of view; nevertheless, they have a T_{1xz}, mainly the intermediate T_{1xz}, which still places them in the NC category. This is qualita-

tively consistent with other authors[29] who find evidence in iPP for, e.g., "rigid amorphous" fractions.

4. Is the Aging Behavior Mainly a Crystallization Phenomenon? Since line shape analysis has shown that aging in iPP apparently converts segments with higher mobility to segments exhibiting the widest line widths (see Figure 4), it is tempting to conclude that aging involves crystallization. However, we now recognize that a nontrivial fraction of the broad-line width component has an intermediate T_{1xz}, indicative of more mobility than would be associated with well-defined crystalline segments. The fact that the changes seen in this aging process only need involve 2–3% of the total number of monomers means that it is possible, in principle, that most of the structures formed might have low mobility but be less than crystalline. What follows is an attempt to clarify this issue by referring to the T_{1xz} behavior of the material that is transformed by aging.

The T_{1xz} profiles, A and B in Figure 8, respectively correspond to iPP-2, originally aged for 49 months and aged for only 30 min following exposure at 89 °C for 6 min. Decay D in Figure 8 is the difference of A − B in Figure 8, where the "0"-level of this difference is coincident with the difference amplitude at the time origin. Having so normalized A and B in Figure 8, the difference, D in Figure 8, can be interpreted as follows: The rapid initial drop corresponds to the fact that Figure 8B contains an excess number of spins with a very rapid T_{1xz} decay. Also, given that the amplitude at the longer time does not return to the "0" level one can infer that 8A has an excess number of spins with the longest T_{1xz}. In fact, decay E in Figure 8 is generated by adding a small amount of the CR−T_{1xz} of C in Figure 8 to the difference, D in Figure 8. From parts D and E in Figure 8, one can conclude that about 75% of the excess fast-decay amplitude in Figure 5B can be mapped into the longest-decay component of Figure 8A, whereas about 25% of the fast decay gets mapped into the intermediate-T_{1xz} component. Thus, *the majority of aging induced structures that were destroyed by the heat treatment at 89 °C fall into the category of "crystalline structures" as defined by their "longest-T_{1xz}" relaxation profiles.*

While Figure 8 illuminates the nature of the changes between long-term aging and heat treatment well below T_m, this is not exactly the same as monitoring structural changes during, e.g., a 4 d aging cycle. However, this plot is also representative of changes in T_{1xz} behavior (not shown) associated with short-term aging over a few days in the iPP-1 sample. The generality of these changes in T_{1xz} is not very surprising in view of the generality of the line shape changes (but not of the fractions of monomers involved) with aging time in both iPP-1 and iPP-2, and in view of the reversibility in the formation and destruction of aged domains with thermal cycling (see Figure 6).

In Figure 8D, the amplitude of the negative-going signal is in excellent agreement with the differences in ordinate values in Figure 6, corresponding to the different aging histories associated with spectra A and B in Figure 8. This is expected when the fast-T_{1xz} component corresponds to the motionally averaged component of the Bloch-decay line shape.

5. Measurements of τ_{null}. The changes in τ_{null} ($= T_1^H/\ln 2$) as a function of τ_{age} are not so easily understood or interpreted. For the originally aged iPP-1, where the τ_{null} values could be determined to an accuracy of ±3

ms, it was found that $T_1{}^H$ decreases about 6%, from 565 ms at τ_{age} = 23 min to 533 ms at 240 min, in a very nonlinear way. After 240 min, a time when only about half of the aging changes have occurred, $T_1{}^H$ quits changing. The initial decrease in $T_1{}^H$ is consistent, at least from the point of view of the direction of change, with the influx of paramagnetic oxygen into the sample following heat treatment in a vacuum. In fact, this hypothesis is borne out by the fact that, when subsequent heat treatments were carried out in air, changes were almost insignificant, i.e., τ_{null} was 534 ms at short aging times compared to the asymptotic value of 532 ms at longer times. The slight increase in τ_{null} at short times could, again, easily be explained by the slight loss of paramagnetic, dissolved oxygen during the heating cycle. For iPP-2, results were similarly constant, i.e., the τ_{null} values were 523 ± 2 ms for all conditions. The primary observation, related to τ_{null} measurements, is as follows: *When thermal treatments are carried out in air, τ_{null}, for any given sample, deviates less than 0.4% and is independent of aging time.*

Discussion

DSC. In one sense, aging at 20 °C is not expected since the NC T_g in iPP is near 0 °C. At the same time, it is probably not correct to assume that all portions of the NC chains have the same T_g. As mentioned in the Introduction, the existence of aging near ambient temperature is not in doubt and has been seen by a variety of techniques. Also, similar aging-induced endotherms are also seen[23] in systems which have expected, broad temperatures of crystallization, such as random copolymers where the homopolymer of the dominant monomer would form a crystalline polymer and where the comonomer is mainly partitioned into the NC regions. Then, at sufficiently high concentrations of comonomer, the comonomer statistics, along with temperature, chain constraints, and the kinetics of local motions, determine the ability of a chain segment to crystallize. In such cases, isothermal aging at temperatures well below the melting point (but above T_g) tends to produce some additional molecular ordering (often described as some type of crystallization), which, in a DSC run, yields an endotherm whose maximum is not far above the aging temperature. Moreover, the temperature of this maximum usually increases with aging time. The breadth of this lower-temperature endotherm (Figure 2) in these iPP's indicates that this aging produces structures exhibiting a range of melting temperatures. The existence of such a temperature distribution is implied in the data of Figure 5 in the sense that the heat treatment at 69 °C produced a mobile fraction smaller than did the heat treatment at 89 °C.

It is significant that when we assume that the low-temperature endotherm comes from crystalline structures having a ΔH_f of 209 J/g, characteristic of the primary crystals, this DSC estimate of the crystallinity change in iPP-1 upon 1 d of aging, (about +0.6%) is about 2.5 times smaller than that deduced from the NMR measurements (+2.0% from Figure 7, modified to about 1.5% by extrapolating the results of Figure 8 to iPP-1). Hence, the implied real ΔH_f of the secondary crystals is approximately 80 J/g, qualitatively consistent with the low melting temperature of these structures. In fact, if one assumed that the secondary crystals had large lateral size the Gibbs−Thomson[45] equation could be rearranged to calculate a minimum stable crystal

thickness l_{min} as

$$l_{min} = \frac{2\sigma_e T_m}{\Delta H_f(T_m - T_m')} \tag{1}$$

where σ_e is the fold crystal/melt interfacial free energy (0.146 J/m²),[46] T_m is the equilibrium melting temperature corresponding to the molecular mass of interest (212 °C),[46] and T_m' is the observed melting temperature (45 °C). This then provides an estimate for l_{min} for the secondary crystallites of 4.3 nm if we use the literature value of the heat of fusion of 209 J/g or 11 nm if the implied real value of the heat of fusion of 80 J/g is used. The applicability of the thermodynamics of chain folded crystallites is certainly questionable for secondary crystals as is the notion that these crystals have lateral dimensions that greatly exceed their thickness and we offer this calculation simply as an example, not to be equated with any bias of our own toward this point of view. However, in the event that lateral dimensions were small or that these crystallites were more like fringed micelles, we would expect that the crystalline stem length in any crystallite, with a melting point of 45 °C would require a stem length longer than that of the Gibbs nucleus (4.3 nm). We will use this minimum length argument later.

Previous NMR Studies Related to Aging in iPP. We are in agreement with Agarwal[27] et al. that aging diminishes the average mobility of the NC regions. Their sample was a Ziegler−Natta product of unspecified molecular weight and defect characteristics; moreover, their thermal treatment, very different from ours, was melt-quenching. Thus, it does not necessarily follow that we should observe similar aging behavior. However, one of their aging temperatures chosen was the same as ours. They noted the NC mobility change only qualitatively. Moreover, they also claimed that crystallinity did not change during aging, a point where we differ. At the same time, they saw a density increase during aging that was linear in log(τ_{age}) and that would fit in very well with a crystallization phenomenon having the same time dependence.

A recent, low-field (26 MHz) proton NMR study[29] of iPP strongly suggests a more heterogeneous structure for iPP than we have assumed here. The sample studied was a Ziegler−Natta product with a polydispersity of 7.6, M_n of 21 700, and an unknown concentration of defects. Those authors identified 2 regions at ambient temperature, with differing $T_1{}^H$ values, ca. 180 and 500 ms. In our samples, the spin diffusion coupling of the CR and NC regions is sufficiently strong (see Figure 10) that the CR and NC regions would have apparent $T_1{}^H$'s different by less than 30 ms. We believe that the iPP studied in that report[29] is not typical of our samples and is more heterogeneous than ours. Thus, we hesitate to adopt their morphological assignments or discuss our samples in terms of all the components they reported.

Proper Definition of Crystallinity. In this paper, we have adopted a definition of crystallinity based on the protons possessing a long T_{1xz}. Moreover, we identify secondary crystallization based on a dominant fraction of transformed material having a long T_{1xz}. We recognize that certain authors[47,48] might dispute whether this is truly a good definition. For example, in melt-quenched samples of mainly metallocene-synthesized iPP's of varying molecular weights and defect concentrations, it was found[48] that density and X-ray estimates of

crystallinity agreed with one another; however, DSC values were lower by 0.15−0.25. This disparity was attributed to the existence of partially ordered interfacial material which material, it was claimed, influenced the X-ray and density measurements but possessed negligible heat of melting. We do not dispute the existence of varying degrees of order within the nominally crystalline material. Certainly, there is good evidence that, at the surface where the chains emerge from the crystallites, the chain packing is not as perfect as in the crystallite interior.[31] Yet, to identify about one-third of these low-mobility chains as "rigid amorphous", or some such designation, seems much too large for an interface. The selection of crystalline chains at ambient temperature, based on their having a long T_{1xz}, is commended for three reasons: (a) T_{1xz} decays are made up of the superposition of individual relaxations without complications from spin diffusion between protons. (b) T_{1xz} is sensitive mainly to motions in the mid-kilohertz regime (therefore, in addition to the long T_{1xz}'s expected for methine and methylene protons in the rigid crystalline regions, the rapidly rotating methyl counterpart-protons will also have long T_{1xz}'s so long as there is no slow wagging of rotation axes). (c) Finally, the sensitivity of T_{1xz} to midkilohertz motions will help to classify residues in defective regions as noncrystalline because small changes in intermolecular potentials lead to increased mobilities at these frequencies. In these iPP's, the decrease in crystallinity by about 10% using a T_{1xz} criterion vs a linenarrowing criterion in Bloch-decay spectra testifies to the greater sensitivity of T_{1xz} to slower motions.

Other NMR criteria have been applied in determining crystallinity by NMR. In a 50-MHz ¹³C NMR study[47] iPP crystallinity was based partly on methylene line shape but mainly on the fraction of methylene carbons having a long longitudinal relaxation time, T_1^C. In that work, about 27% of the methylene carbons in a slowly crystallized Ziegler−Natta iPP, from which the amorphous component had been removed, were assigned by the authors to a defective interfacial region where the chains probably had helical conformation but, on the basis of T_1^C, could still be regarded as less than crystalline. In contrast, their so-called NC fraction was similar to the fraction of protons that showed motional averaging in our samples. However, we only added about 10% (not 27%) to our NC fractions by moving away from a "motional-averaging" definition of the NC fraction to a "short-plus-medium-T_{1xz}" definition. Thus, we would expect that some of our "long-T_{1xz}" protons (="CR" protons) would be situated in regions those authors would still consider less than crystalline. Despite the above arguments and interpretations, we are, as yet unwilling to concede that such large interfaces typically exist in iPP, and would further argue that the "long-T_{1xz}" criterion is a competitive candidate for defining crystallinity in iPP. We cite a couple of reasons. First, regarding the long-T_1^C definition, the methylene T_1^C can be perturbed to a modest extent, by ¹³C−¹³C spin exchange[49] with more rapidly relaxing ¹³C-methyl carbons which occupy 1.1% of the methyl sites. This spin exchange interaction falls off as the inverse sixth power of the ¹³C−¹³C internuclear distance; hence the number of methylene carbons influenced, in a natural abundance sample, is statistically determined; however, that fraction is not negligible and contributes to an underestimate of crystalline fraction, using this T_1^C criterion.

Also, certain assumptions about component line shapes were made in the T_1^C analysis and that could have influenced component size. As to the notion that DSC gives a good measure of crystallinity in melt-quenched samples, there is a question about the appropriate ΔH_f, given that (a) there are different levels of suggested crystalline organization possible in the α-phase crystals of iPP, including, at the most discriminating level, the directional ordering[50,51] of adjacent chains in the lattice. Moreover, it is now recognized[31] that chain defects are partially incorporated into the CR lattice and there will be some corresponding impact on lattice heat content for those inclusions as well. Thus, especially for iPP samples that have been melt-quenched, DSC may significantly underestimate the amount of material that has lattice character and should be regarded as crystalline.

The Morphological Location of Secondary Crystallization. The exact location for secondary crystallization is not clear from these experiments, nor is the type of structure formed during this crystallization very apparent. Could these be new, small, crystalline entities, such as fringed micelles? Or are segments, with, e.g., shorter and shorter stem lengths and greater and greater topological constraints (to explain the slowing crystallization kinetics and the broad melting behavior) sequentially laying down *on the faces* of existing crystallites? Or could all of this crystallization be occurring near spherulitic boundaries? One thing seems clear from the reversibility of the melting behavior in Figure 6, namely, that one is **not** thickening the stems of the main crystallites, since such a process would lead, contrary to observation, to crystalline structures stable below the main melting endotherm near 160 °C. It has been pointed out[23] that one of the signatures of chain-folded crystallites is that there is a temperature hysteresis between the crystal formation temperature and the crystal melting temperature. This point is then used to argue that, in secondary crystallization, when one does not see such hysteresis, chain folding is absent and in its place, something like "fringed micelles" or "chain-cluster-like" crystals form.[23] In the observations we have made, relative to the possibility that fringed micelles form, our data are consistent with but do not prove this type of structure. The reversibility seen in Figure 6 only tells us that aging-induced crystallization at 20 °C, following a heating period at 89 °C, contributes negligibly to structures having a thermal stability greater than 89 °C.

There are two observations that *may* present clues about the positioning of the crystals formed by secondary crystallization. First is that the line width of the NC component that is lost as secondary crystallization proceeds (Figure 4C) implies that the population of NC segments with higher-than-average mobility is most affected by the aging process. If mobility increases as one moves away from the surfaces of the primary crystallites, then this loss could suggest that the segments participating in secondary crystallization mainly come from the regions furthest from those CR surfaces. (Here we are thinking more of those surfaces out of which chains emerge, rather than lateral surfaces; the former are assumed dominant for the primary crystallites.) We are cognizant, however, that the reduction in the number of higher-mobility segments may also be the result of slightly reducing the mobility of *all* NC segments upon secondary crystallization, assuming that

these NC segments possess a wide mobility distribution at any given time. Then, it would only *appear* as if the more mobile segments were the main participants in the process, since there are no populations to replenish the most mobile population. Yet, the fact (see Figure 3H) that the line width of the more mobile participating segments does not change during the first and second halves of the 4 d aging seems to discount the notion that all NC segments slowly lose mobility as aging progresses. By default, this elevates the probability that the more mobile segments are actually those converted to crystalline segments during aging. So we regard the foregoing mobility considerations as a *weak* argument favoring the notion that secondary crystallization happens far away from the existing faces of chain-folded crystals.

The second observation, possibly related to the morphological location of the secondary crystallization, is the lack of any aging effect on τ_{null}. The observation that τ_{null}, and, by implication, T_1^H, is independent of aging time is not necessarily in accord with the postulate that the NC protons have a significantly shorter intrinsic T_1^H than do their CR counterparts. At the same time, given the ^{13}C longitudinal relaxation times reported[47] for iPP segments in various morphological regions, there is little doubt that this postulate holds for iPP. Thus, the overall T_1^H should, be strongly influenced, via spin diffusion, by the intrinsic T_1^H of the NC protons. As mentioned previously, iPP is a bit more complicated because methyl rotation in the CR region makes the CR contribution to relaxation nonnegligible in iPP; nevertheless, the more facile motions of the backbone protons in the NC regions make its intrinsic T_1^H significantly shorter than that of the CR protons. During a 4 d aging period in iPP-1, about 7−9% of the NC chains crystallize. Naively, one might expect this reduction in the number of NC protons to produce a change in τ_{null} of at least a few percent, even if the intrinsic T_1^H for the CR protons were only twice that of the NC protons.

One possible explanation for the constant T_1^H is morphologically uninteresting, namely, that at the longer τ_{age} values, the loss in the number of NC segments is offset by a change in average NC mobility. The implication is that secondary crystallization exerts a widespread influence on the NC chains in such a way that the T_1^H of the average NC proton is reduced by an amount that exactly cancels the effect of losing some NC protons. As just noted, however, there is reason to be skeptical that aging produces a generalized reduction in mobility for all NC segments.

A second possible explanation for the constancy of T_1^H is morphologically more intriguing. If we assumed that the intrinsic T_1^H's for the NC and CR remained constant, then, one would have to find some way that the secondary crystallites that form would have a minimal impact, via spin diffusion, on the relaxation of the protons in the primary crystallites. The easiest way to accomplish this is to keep the secondary crystallites more distant from the primary crystallites. As an initial perspective on how that might be accomplished, recall that we had earlier calculated the stem length of 4.3 nm (or 11 nm for the "corrected" heat of fusion) for a stable nucleus with a melting point of 45 °C and that we regarded this length as a minimum, associated with any nucleus that would form. Consider also that from the data of Figure 10 the typical NC thickness is about 7 or 8 nm. Finally, consider that the amount of secondary crystallites that form over a 4 d period represents

only 2% or 3% of the total volume of material. Then, if the secondary crystallites are widely dispersed throughout the NC regions between the primary crystallites, the most likely scenario with the least impact on the overall T_1^H is to have many crystallites, very small in lateral dimensions, near the centers of the NC domains, and probably oriented so that their stems are closer to being orthogonal to the stems of the primary crystallites. At the other morphological extreme, where secondary crystallites are envisioned to have substantial lateral dimensions, one would be limited to finding the secondary crystallites in a few, larger NC regions that are devoid of primary crystallites ... and this could include regions like spherulitic boundaries. From an NMR point of view, we have no reason to prefer a scenario with smaller or larger lateral dimensions for the secondary crystallites. However, if aging involved the nucleation of just a few sites vs the nucleation of numerous small crystallites, one might be able to interpret more clearly the processes that yield the logarithmic growth of secondary crystals with τ_{age}, as well as the typical parallel increase in average melting temperatures of these crystals.

The possibility that secondary crystallization might be located in, e.g., spherulitic boundaries as opposed to being more widely distributed over NC sites, was one motivating influence in our choice of iPP-2. Since the Ziegler−Natta-polymerized iPP-1 was expected to have a noncrystallizing amorphous component,[44] in addition to having a significantly larger polydispersity and a slightly higher level of chain defects (vide infra) compared with iPP-2, there were many reasons to expect that a nontrivial amount of material could be segregated to spherulitic boundaries during the relatively slow melt crystallization of iPP-1. Candidate chains for such segregation are much less numerous for the iPP-2 sample. Yet, in terms of the fraction of material involved in aging following the 89 °C thermal treatment, iPP-2 aging involved about 72% as many sites over a given aging time as were involved in iPP-1 aging (see Figure 7). Thus, while the extent of secondary crystallization may still somehow depend on the density of defects or the polydispersity, the fraction of chains that might segregate to the spherulitic boundaries does not seem to be the controlling consideration. Thus, we view the considerations in this paragraph as *lowering*, not raising, the probability that secondary crystallization in iPP should be limited to spherulitic boundaries.

Regarding the Fraction of iPP Involved in Secondary Crystallization. If secondary crystallization is not associated with spherulitic boundaries, then what does control the amount of such crystallization? Perhaps polydispersity or defect levels are important. However, relative to iPP-1, iPP-2 has significantly lower levels in both categories; yet, as noted in the previous paragraph, the ratio of the amounts involved in secondary crystallization is quite high. Thus, although we cannot demonstrate this conclusively*, we expect that even a defect-free sample of modest polydispersity would show aging of the kind seen here.*

Relative to the amount of amorphous material that can be identified in the proton Bloch-decay spectra, a spectral comparison of comparably aged samples of iPP-1 and iPP-2 showed that at 10 min after an 89 °C heating, the excess narrower intensity that iPP-1 displayed over that of iPP-2 corresponded to only 3.6% of the total intensity. After 4 d of aging, this excess became

2.9%, owing to the greater fraction converted by aging for iPP-1. Therefore, *an upper limit on the fraction of noncrystallizable chains in iPP-1 is about 3%,* assuming that the iPP-2 has none of these chains. It is also notable that the line width associated with this excess narrower intensity was in the range 6−7 kHz, considerably wider than the 4.3 kHz line width associated with the NC component that disappears upon aging and narrower than the 10.5 kHz width for the typical motionally averaged NC protons (see Figure 9). Thus, if the excess narrower intensity of the iPP-1 sample arises from noncrystallizable-chain protons, it makes sense that these protons would have mobilities higher than is typical of NC protons; however, these line widths are not so narrow as 4.3 kHz, a value that might otherwise tempt us to assign secondary crystallization to crystallizable chains in a region possibly shared with noncrystallizable chains.

Chain segments with statistically higher defect concentrations are always candidates for delayed, lower-temperature crystallization. The defect concentration in iPP-2 has been determined and it is relatively low, i.e., 0.41 mol %. No similar high-resolution NMR analysis was applied to the iPP-1 sample. Yet, we can make a crude estimate of the defect content in iPP-2 based on the relative strengths of the stereodefect resonances in the CPMAS spectra (not shown) of the CR region for the iPP-1 sample relative to defect-resonance intensities for other iPP's with known stereodefect contents.[31] If we compare to a metallocene-synthesized iPP, the stereodefect content for iPP-1 *for the crystallizable chains* (at least 97% of the chains) would be 1.0 ± 0.3 mol %. However, given the partial suppression of CR defect content in Ziegler−Natta-polymerized iPP's relative to metallocene-polymerized iPP's,[31] a conservative estimate of stereodefect content for the crystallizable chains in iPP-1 is 1.6 ± 0.5 mol %, somewhat higher than the defect content of iPP-2. It is not a foregone conclusion in this case that a higher defect content in iPP-1, relative to iPP-2 automatically means that more secondary crystallization can occur in iPP-1. With a higher defect concentration, there are more segments excluded from primary crystallization; hence, there is a larger reservoir of NC chains. However, the ability to form stable secondary crystallites is a combination of (a) the number of amorphous stems that have qualifying, defect-free lengths greater than some minimum, temperature-dependent value *and* (b) the ability of those stems to come together, given the chain constraints arising from incorporation of other portions of the chain into primary crystallites. This is a complex problem, beyond the scope of this paper. We only comment that, given the typical heterogeneous distribution of defects in Ziegler−Natta iPP's, we are not comfortable in declaring whether the difference in defect levels in iPP-1 vs iPP-2 should result in an increase or decrease in the amount of secondary crystallization of these qualifying stems.

Advantages and Generality of this NMR Method for Studying Aging. The fact that we can both see and quantify aging events that affect only a few percent of the total segments speaks to the sensitivity of the method. For the iPP samples studied, the sensitivity exceeds that of DSC, especially if normal-sized DSC samples are used. Clearly, this NMR method, if carried over to other polymers, would generally depend strongly on there being some motional averaging that is helping to distinguish the more mobile from the more rigid protons. In other words, the aging-analysis temperature should be well above the NC T_g. Aside from sensitivity issues, the NMR method gains advantage simply because it is nondestructive of the aging process. Thus, in contrast to DSC, the NMR approach can eliminate sample-to-sample variations or can eliminate cumulative effects resulting from repeated thermal cycling if one wishes to follow an aging process. Finally, one can also pursue other issues such as whether the aging process produces actually crystalline material or just defective, rigidified regions.

Conclusions

Ambient temperature aging in iPP, after mild thermal cycles, has been followed, with sensitivity superior to DSC, using carefully analyzed changes in the proton Bloch-decay spectra. That the aging process can be viewed primarily as secondary crystallization, rather than a generalized densification of the noncrystalline (NC) stems, is supported by both line width and T_{1xz} criteria, the latter being a more stringent criterion in the sense that it is sensitive to slower motions than the line width would be. The minimum fraction of repeat units whose motions are strongly modified during, e.g., a 4 d aging period after a heating cycle to 89 °C, is relatively small, i.e., about 0.02 for a low-defect metallocene iPP and about 0.03 for a Ziegler−Natta iPP with slightly higher defect content and significantly greater polydispersity. Over the range from about 6 min to 4 d of aging time, the growth of secondary crystals is linear in the logarithm of aging time. An attempt to associate a modified heat of fusion with the secondary crystallites formed by aging, using DSC data, suggested a value about 40% that of the pure iPP crystal. Consistent with this low heat of fusion, the DSC also indicated that the aging-induced structures that formed at ambient temperature would be destroyed again upon heating to the original heat-treatment temperature (89 °C).

Although we were searching for clues about (1) the *morphological location* of the secondary crystallization and (2) any chemical or microstructural issues that would influence the *amount of* secondary crystallization, we could, in the end, say nothing definitive, other than that secondary crystallization was definitely not adding to the perfection of the primary crystals. Interesting observations which still await proper connection to these issues are the following: (a) The population of NC chains most strongly decimated in the aging process is that of the most mobile, NC chains. This observation raises the possibility, but does not prove, that secondary crystallization is taking place primarily in regions of highest mobility that are more distant from the fold surfaces of the primary crystallites. (b) Even though the fraction of NC chains is being reduced by secondary crystallization, the longitudinal proton relaxation time, T_1^H, a parameter that is usually sensitive to the fraction of NC chains, remains puzzlingly constant throughout the aging process as though the local ratio of crystalline to NC stems were remaining constant at most sites. This *might* suggest that the spatial dispersion of secondary crystals is more coarse-grained relative to the dispersion of primary crystals (assuming that the secondary crystallites have larger lateral dimensions) or that the dispersion of these crystallites is widespread and peppered throughout the NC regions (assuming crystallites of very small lateral dimension). While the possibility

was considered that secondary crystallization was mainly occurring near spherulitic boundaries, involving more defective, or lower-molecular-mass molecules, the relatively large amount of secondary crystallization associated with iPP-2, relative to iPP-1, was considered as an argument against such a simple view. Many questions remain.

References and Notes

(1) Struik, L. C. E. *Plast. Rubber Proc. Appl.* **1982**, *2*, 41−50.
(2) Struik, L. C. E. *Polymer* **1987**, *28*, 1521−1533.
(3) Struik, L. C. E. *Polymer* **1987**, *28*, 1534−1542.
(4) Struik, L. C. E. *Polymer* **1989**, *30*, 799−814.
(5) Struik, L. C. E. *Polymer* **1989**, *30*, 815−830.
(6) Chai, C. K.; McCrum, N. G. *Polymer* **1980**, *21*, 706−712.
(7) McCrum, N. G. *Polymer* **1984**, *25*, 299−308.
(8) Isasi, J. R.; Mandelkern, L.; Galante, M. J.; Alamo, R. G. *J. Polym. Sci., Polym. Phys. Ed.* **1999**, *37*, 323−334.
(9) Zhou, H.; Wilkes, G. L. *Polymer* **1997**, *38*, 5735−5747.
(10) Kong, Y.; Hay, J. N. *Polymer* **2002**, *43*, 3873−3878.
(11) Ruland, W. *Acta Crystallogr.* **1961**, *14*, 1180−1185.
(12) Baltá-Calleja, F. J.; Vonk, C. G. *X-ray Scattering of Synthetic Polymers*; Elsevier: New York, 1989.
(13) Olley, R. H.; Bassett, D. C. *Polymer* **1989**, *30*, 399−409.
(14) Mansfield, M.; Boyd, R. H. *J. Polym. Sci., Polym. Phys. Ed.* **1978**, *16*, 1227−1252.
(15) Mansfield, M. L. *Chem. Phys. Lett.* **1980**, *69*, 383−385.
(16) Skinner, J. L.; Wolynes, P. G. *J. Chem. Phys.* **1980**, *73*, 4015−4021.
(17) Skinner, J. L.; Park, Y. H. *Macromolecules* **1984**, *17*, 1735−1740.
(18) Syi, J.-L.; Mansfield, M. L. *Polymer* **1988**, *29*, 987−997.
(19) Boyd, R. H. *Polymer* **1985**, *26*, 323−347.
(20) Boyd, R. H. *Polymer* **1985**, *26*, 1123−1133.
(21) Spiess, H. W.; Schmidt-Rohr, K. *Macromolecules* **1991**, *24*, 5288−5293.
(22) Hu, W.-G.; Boeffel, C.; Schmidt-Rohr, K. *Macromolecules* **1999**, *32*, 1611−1619.
(23) Alizadeh, A.; Richardson, L.; Xu, J.; McCartney, S.; Marand, H.; Cheung, Y. W.; Chum, S. *Macromolecules* **1999**, *32*, 6221−6235.
(24) Marand, H.; Alizadeh, A.; Farmer, R.; Desai, R.; Velikov, V. *Macromolecules* **2000**, *33*, 3392−3403.
(25) Alizadeh, A.; Sohn, S.; Quinn, J.; Marand, H.; Shank, L. C.; Iller, H. D. *Macromolecules* **2001**, *34*, 4066−4078.
(26) Kramer, H.; Helf, K. E. *Kolloid Z.* **1962**, *180*, 114−118.
(27) Agarwal, M. K.; Schultz, J. M. *Polym. Eng. Sci.* **1981**, *21*, 776−781.
(28) Yue, C. Y.; Msuya, W. F. *J. Mater. Sci. Lett.* **1990**, *9*, 985−988.
(29) Weglarz, W. P.; Peemoeller, H.; Rudin, A. *J. Polym. Sci., Polym. Phys. Ed.* **2000**, *38*, 2487−2506.
(30) Certain commercial companies are named in order to specify adequately the experimental procedure. This is no way implies endorsement or recommendation by the authors or their agencies.
(31) Vanderhart, D. L. Nyden, M. R.; Alamo, M.-H. Kim, R. G.; Mandelkern, L. *Macromolecules* **2000**, *33*, 6078−6093.
(32) Annual Book of ASTM Standards, Vol. 08.02, 6474−99.
(33) Private communication from the probe manufacturer, Doty Scientific, Inc.
(34) Farrar, T. C.; Becker, E. D. *Pulse and Fourier Transform NMR*; Academic Press: San Diego, CA, 1971; pp 20−21.
(35) Waugh, J. S.; Huber, L. M.; Haeberlen, U. *Phys. Rev. Lett.* **1968**, *20*, 180−182.
(36) Rhim, W.-K.; Elleman, D. D.; Vaughan, R. W. *J. Chem. Phys.* **1973**, *59*, 3740−3749.
(37) Mansfield, P.; Orchard, J.; Stalker, D. C.; Richards, K. H. B. *Phys. Rev.* **1973**, *B7*, 90−105.
(38) Vega, A. J.; Vaughan, R. W. *J. Chem. Phys.*, **1978**, *68*, 1958−1966.
(39) Abragam, A. *The Principles of Nuclear Magnetism*; Oxford University Press: Oxford, England, 1961; Chapter V.
(40) VanderHart, D. L.; McFadden, G. B. *Solid State Nucl. Magn. Reson.* **1996**, *7*, 45−66.
(41) Havens, J.; VanderHart, D. L. *Macromolecules* **1985**, *18*, 1663−1676.
(42) Krigbaum, W. R.; Uematsu, I. *J. Polym. Sci., Polym. Chem. Ed.* **1965**, *3*, 767−776.
(43) Hamada, F.; Nakajima, A. *Kobunshi Kagaku* **1965**, *22*, 577−583.
(44) Randall, J. C. *Macromolecules* **1997**, *30*, 803−816.
(45) Hoffman, J. D.; Davis, G. T.; Lauritzen, J. I., Jr. In *Treatise on Solid State Chemistry*, Hannay, N. B., Ed.; Plenum Press: New York, 1976; Vol. 3; Chapter 7.
(46) Xu, J.; Srinivas, S.; Marand, H.; Agarwal, P. *Macromolecules* **1998**, *31*, 8230−8242.
(47) Saito, S.; Moteki, Y.; Nakagawa, M.; Horii, F.; Kitamaru, R. *Macromolecules* **1990**, *23*, 3256−3260.
(48) Isasi, J. R.; Mandelkern, L.; Galante, M. J.; Alamo, R. G. *J. Polym. Sci., Part B, Polym. Phys.* **1999**, *37*, 323−334.
(49) VanderHart, D. L. *J. Magn. Reson.* **1987**, *72*, 13−47.
(50) Hikosaka, M.; Seto, T. *Polym. J.* **1973**, *5*, 111−127.
(51) Mencik, Z. *J. Macromol. Sci. Phys.* **1972**, *B6*, 101−115.